A Uniform Residence Time Flow Cell for the Microreactor-Assisted Solution Deposition of CdS on an FTO-Glass Substrate

B. K. Paul,*,[†] C. L. Hires,[†] Y.-W. Su,[‡] C.-H. Chang,[‡] S. Ramprasad,[§] and D. Palo[§,||]

[†]Oregon Process Innovation Center/Microproducts Breakthrough Institute, School of Mechanical, Industrial and Manufacturing Engineering, Oregon State University, Corvallis, Oregon 97330, United States

[‡]Oregon Process Innovation Center/Microproducts Breakthrough Institute, School of Chemical, Biological and Environmental Engineering, Oregon State University, Corvallis, Oregon 97330, United States

[§]Oregon Process Innovation Center/Microproducts Breakthrough Institute, Pacific Northwest National Laboratories, Corvallis, Oregon 97330, United States

ABSTRACT: Photovoltaic cells have long been a desirable alternative to the consumption of fossil fuels, but current manufacturing practices suffer from poor energy efficiency, large carbon footprints, low material utilization, and high processing temperatures. A critical step in production of thin film CdTe and $CuInSe_2$ solar cells is the chemical bath deposition of a CdS thin film to serve as a "buffer layer" between the optically absorbent layer and the transparent conducting oxide. In prior work, functional CdS films were demonstrated at low temperature using a continuous flow, microreactor-assisted deposition process showing good selectivity of heterogeneous surface reactions over homogeneous bulk precipitation. In this paper, we develop a flow cell for implementing a uniform CdS film over a 152 mm substrate. Analytical models are coupled with computational fluid dynamic simulations to design a flow cell with more uniform flow fields. Experimental results demonstrate a 12% coefficient of variance for a 21.5 nm thick film.
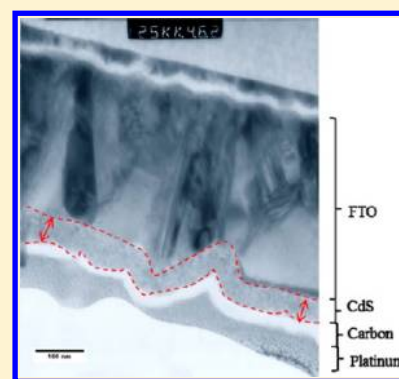
INTRODUCTION

Cadmium sulfide (CdS) is often used to form the junction of a heterojunction thin film photovoltaic (PV) cell.[1,2] It serves to form the p−n junction and extend the distance photocarriers can travel before recombination can occur and to reduce reflection in the absorber layer of the cell.[3] Methods that have been explored for CdS deposition include vapor phase techniques, such as physical and chemical vapor phase deposition (PVD and CVD) and liquid phase processes, such as chemical bath deposition (CBD), electrochemical deposition, and successive ionic layer adsorption reactions. Of these methods, CBD is typically valued as the industry standard due to its relative ease of implementation, low temperatures (<100 °C), atmospheric pressures, and consequent low expense for covering large surface areas.

The typical CBD process utilizes a large volume of reaction fluid that is not in intimate contact with the substrate surface, leading to a high volume-to-surface area ratio. This arrangement provides conditions for spatially uniform film growth rates across the substrate area but also results in low yields of cadmium conversion to the final film due to precipitation of CdS in the bulk solution. The unwanted precipitates and byproducts can settle on the film, interrupting the coherency of the film. Additionally, the reagent concentrations decrease over time in a static bath, causing the reaction conditions and growth rate to vary in a temporal manner.

Microreactor-assisted solution deposition (MASD) is the coupling of microreactor technology with continuous flow deposition to resolve the temporal evolution of reaction chemistry. Under continuous flow conditions, byproducts and precipitates can be swept through the reaction chamber and reaction conditions can be kept constant and optimized with respect to time.[4] It has been shown that microreactors can improve material yield and decrease solvent usage in comparison to typical CBD reactor conditions.[5−7] Prior work showed results from a continuous flow microreactor using mL/h flow rates to increase the efficiency and conversion of $[Zn^{2+}]$ to ZnO nanowires.[8,9] This occurs due to the greatly reduced diffusion times experienced in submillimeter diameter channels. Interference pattern measurements showed spatial variation in the ZnO nanowire length due to faster growth near the inlet of the reaction chamber and slower growth near the end as the bulk fluid neared depletion of active species. In addition, a distinct parabolic growth rate pattern can be seen as the fluid traveled faster down the axial center regions in comparison to the outer edges of the reactor. They also inverted the positioning of their flow cell, placing the substrate on the top surface to allow precipitating species to settle away from the growing ZnO wires.

In this paper, we report the development of a high flow rate continuous flow MASD reactor to deposit CdS films over large substrates that compensates for lateral flow variation across a single high-aspect-ratio flow cell. Although much prior work has

been performed to control flow maldistribution across an array of parallel channels, little work has been performed to address flow uniformity across a single high-aspect-ratio channel. Chung et al.[10] designed inlet ports with sizable prereservoir chambers that showed good lateral flow uniformity across a submillimeter cell culture cultivation chamber. However, this approach suffered from increased dead zone regions in the reservoir chamber. An alternative design by Hung et. al[11] effectively split a single inlet into multiple perfusion channels arranged in a semicircular pattern. The total surface area of each perfusion channel was designed to be much smaller than the original inlet port area. The increase in pressure drop across each perfusion channel was designed to regulate flow between channels.

The approach taken in this paper is to manipulate the cross-sectional area of the reaction chamber in a manner to compensate for the variation in travel length based on flow streamlines. This is done by increasing the resistance to flow near the axial center region of the flow cell by deflecting the upper surface into the reaction chamber, thus reducing the channel height in that region.

FLOW CELL DESIGN

The design of a solution flow cell for depositing thin films with uniform thicknesses requires control of deposition both in the breadth and in the length of the flow cell. The flow cell consists of an inlet header, a deposition region, and an outlet header. In this work, triangular inlet and outlet headers were used to connect the inlet and outlet to the deposition region. The size of the inlet header was minimized to eliminate dead volume prior to deposition while efforts were made to minimize backpressure in the outlet header by reducing the angle of convergence. Consequently, the outlet header was found to be larger than the inlet header.

The rationale for the design of the deposition region was as follows. Assuming uniform temperatures within the flow cell, control over film thickness along the axial length of the deposition region has to do mainly with avoiding depletion of reactants by balancing reagent concentration and residence time within the deposition region. Assuming that reagent concentrations are uniform within the flow, control over film thickness uniformity in the breadth of the deposition region has to do mainly with a uniform velocity profile across the breadth of the region. The velocity profile not only affects the residence time of reagents across the deposition region but also determines the thickness of the fluid boundary layer through which reactants diffuse.

Many researchers have looked at ways to distribute or otherwise control flow velocity across headers and microchannels.[12−16] In the deposition region, we applied the approach taken by Pan et al.[17] to optimize the inlet and outlet header design for a microchannel array to minimize the variation of flow distribution across the array by modeling the array as a complex system of flow resistances arranged in series and parallel. For analysis purposes, the flow cell deposition region of the flow cell, consisting of a single high-aspect-ratio flow cell channel (0.8 mm deep × 152 mm wide), was represented as an array of imaginary parallel channels. The pathway and length of each of these imaginary channels were determined by flow streamlines generated using tracer particles within computational fluid dynamics (CFD; Fluent, version 6.3, using GAMBIT as meshing tool) simulations, as shown in Figure 1.

As a first approximation, assuming equivalent pressure drop and velocity within each channel, the relationship between
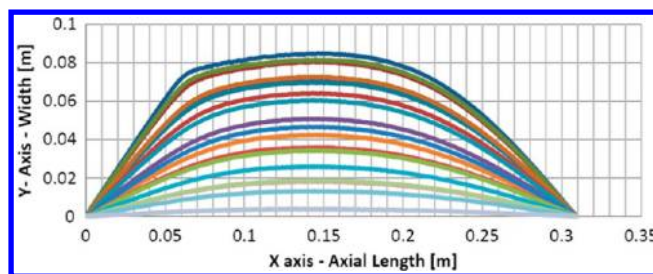

Figure 1. Computer-simulated streamline pathways generated by releasing and tracing point particles from the flow cell inlet to outlet (half model shown).

channels reduces to a ratio of the pathway length to the square of the hydraulic diameter. To simplify the analysis, each imaginary channel was assumed to have a constant submillimeter width. Using channel lengths represented by the streamlines in Figure 1, hydraulic diameters were calculated for each streamline, leading to an initial cross-sectional profile for the flow cell. A cartoon of a deflected channel profile in the deposition region of the flow cell is shown in Figure 2.
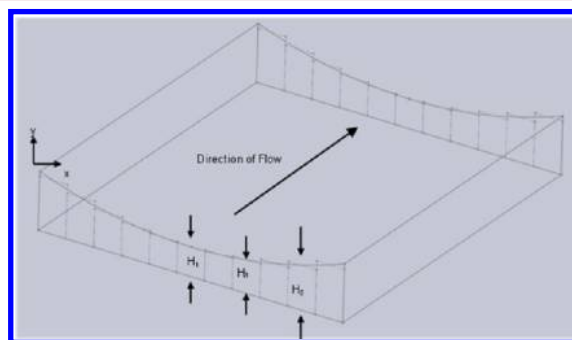

Figure 2. Cartoon of a deflected cross-sectional channel profile showing the need to change the hydraulic diameter as a function of breadth to achieve equivalent velocities or residence time within each individual channel.

COMPUTATIONAL FLUID DYNAMIC SIMULATIONS

To refine the cross-sectional channel profile of the flow cell, CFD simulations were used to evaluate the effect of the channel profile on flow front development and flow distribution within the deposition region. Flow cell cross sections were constructed in SolidWorks 2010. The baseline case to which all deflected-plate results were compared was the condition of two perfectly parallel plates set 800 μm apart. The flow chamber geometry was imported into Fluent, and a three-dimensional CFD analysis was performed. Two-dimensional triangular meshes were generated on the base surface, and the channel depth was partitioned into 10 segments, resulting in 1 763 700 total elements. The boundary conditions for the simulation consisted of no-slip conditions at the flow cell walls and atmospheric pressure at the outlet. Water with a density and viscosity of 9.98×10^2 kg/m^3 and one cP, respectively, was used as the fluid. While the properties of water do not precisely match those of the precursor solution, it was expected that water would closely simulate the flow behavior of the precursor solution. An inlet velocity of 0.089 m/s was calculated from an inlet area of 5.85 mm^2 and a volumetric flow of 31 mL/min. Laminar flow conditions were used at the inlet with a Re of 1 211. Residual values for mass and momentum at convergence were below 1×10^{-5} g and 1×10^{-4} g m/s, respectively (Figure 3).

Flow uniformity was evaluated by tracking the flow front across the flow cell. Fluent was used to simulate the pulse injection of 100 point particles and track their position over the progress of time. Flow front
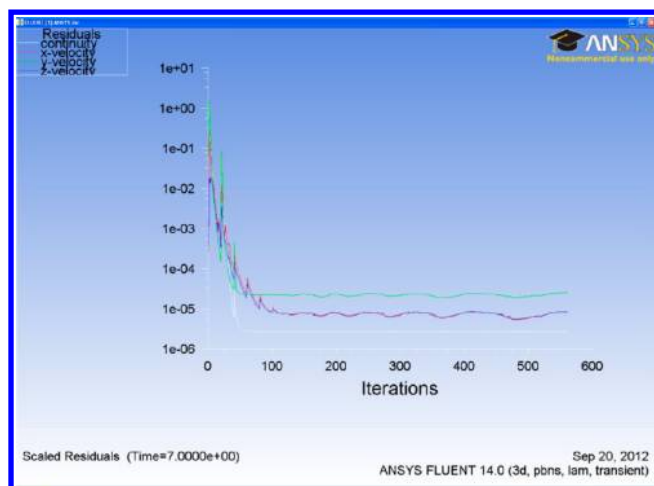
Figure 3. Residual convergence of mass and momentum for a simulated system of discretized equations.

uniformity was evaluated by monitoring the position of these particles along the front edge of the pulse injection, as seen in Figure 4.

The standard deviation of the flow front position was evaluated as it moved through the flow cell using the position of all tracer particles on the flow front as it passed the front, middle, and back planes of the substrate (Figure 5). The standard deviation for the flow front within the parallel-plate flow cell increased from 7.7 to 25.5 mm from the front plane to the back plane. This is due to the distinctive parabolic profile along the front edge of the tracer particles caused by laminar flow conditions. Results show that this parabolic profile becomes more pronounced with time, suggesting that fluid flow is much faster along the center axis of the flow cell, as expected.

To improve the flow front profile, several deflected-plate profiles were produced using finite element analysis (Cosmos) to simulate the method to be used to create the upper deflected plate in the physical experiment. As discussed below, the deflected plates were produced in our experiments using a flow cell fitted with a pattern of set screws that could individually place point loads at different places on the top plate of

the flow cell (Figure 10). The goal of the finite element analyses (FEAs) was to determine the position of point forces needed to closely match deflected channel profiles of promise. For FEA, material properties of the flow cell were input into the Cosmos model and forces were applied at various positions along the central axis and elsewhere. Resultant channel profiles were evaluated in CFD until channel profiles providing the best constant velocity profile within the deposition region of the flow cell were identified. The simulated flow front response for the final deflected profile is shown in Figures 6 and 7. The final deflected-plate profile required roughly 200 μm of deflection along the centerline of flow cell. The final channel profile used in CFD and per the experimental setup is compared in Figure 15 below.

■ EXPERIMENTAL APPROACH

A schematic of the final flow cell experimental setup is shown in Figure 8. Reagents were fed into a microchannel T-mixer using positive displacement pumps (Acuflow Series III). This mixed stream was then fed into a heat exchanger to bring the reactants to temperature and hold for a specific induction time before being introduced into the CdS film deposition flow cell. The flow cell accommodated a glass substrate and contained an integrated heating system to maintain a uniform substrate temperature throughout the fluid residence time. Excess reagents and byproducts were collected into a waste container beyond the flow cell outlet. A LabVIEW program was used for system control and for data acquisition during the experiments. A more detailed description of the test setup surrounding the flow cell is provided elsewhere.[18]

The flow cell assembly developed for deposition of CdS is shown schematically in Figure 9. It consists of a five-layer stack beginning with a 376 × 256 × 6.4 mm thick 6061 T651 aluminum (Al) base plate on which is placed an equally sized 3 mm thick FTO-coated glass substrate. Kapton tape was used to mask the glass for 152 × 152 mm deposition. A thin layer of thermal adhesive was applied between the based plate and glass substrates to aid in heat transfer and temperature control. The geometry of the reaction chamber is then defined by a double stack of 800 μm thick highly compressible closed cell silicone foam (Bisco HT-800). The upper surface of the reaction chamber consists of a 3.18 mm thick polycarbonate (PC) sheet with inlet and outlet ports. This was topped by a secondary 12.7 mm top PC plate fitted with complementary
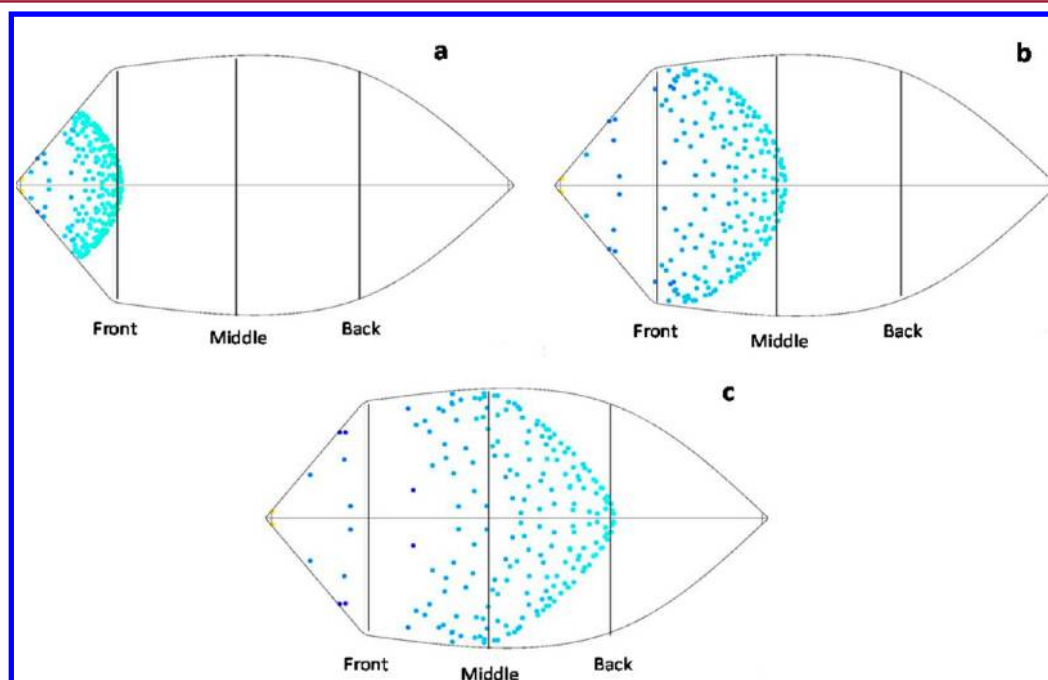

Figure 4. Flow front progression for baseline parallel plates at a depth of 800 μm. Flow distribution for tracer particles when they reach the (a) front plane, (b) middle plane, and (c) back plane.
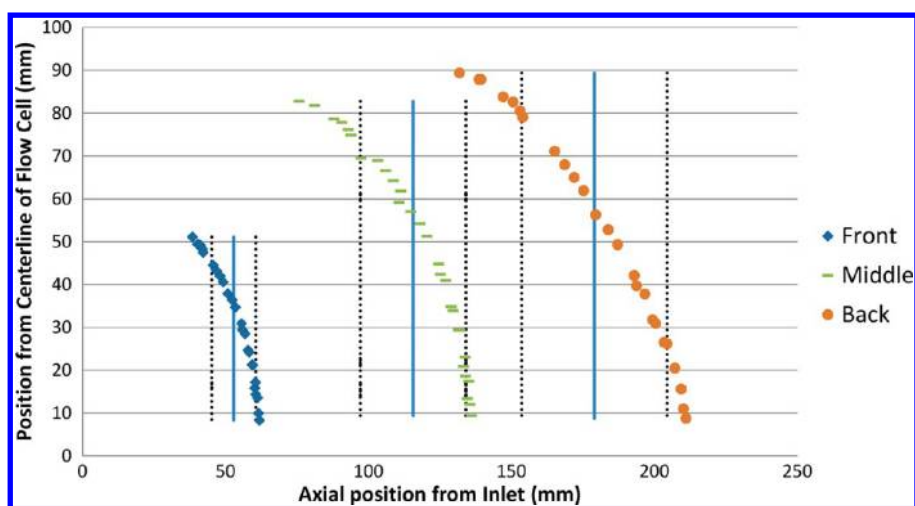
Figure 5. Standard deviations of flow front for baseline parallel-plate channel profile at a depth of 800 μm for front plane = 7.7 mm; middle plane = 18.5 mm; and back plane = 25.5 mm (shows half of flow field from center axis).

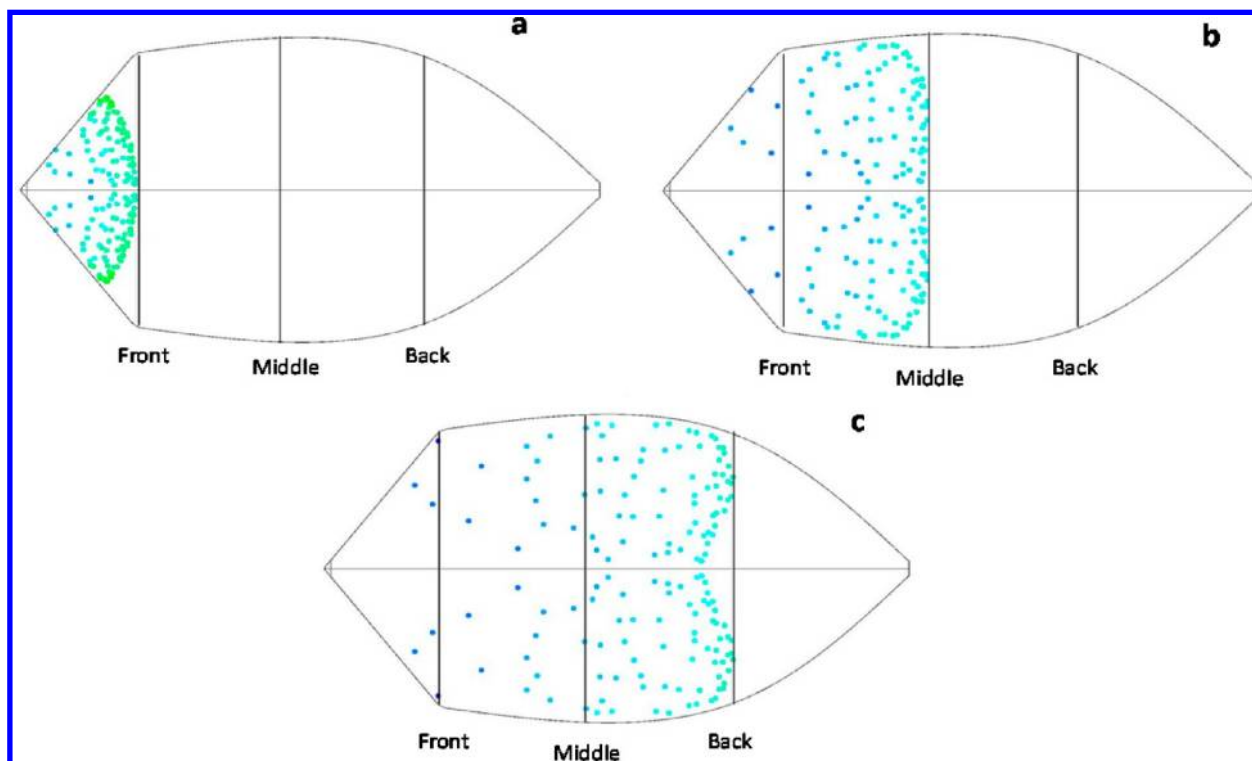**Figure 6.** Flow front progression for deflected-plate channel profiles roughly 600 μm high along the flow cell centerline and 800 μm high along the edge of the flow cell. Flow distribution for tracer particles when they reach the (a) front plane, (b) middle plane, and (c) back plane.

inlet and outlet ports. Seals between plates were made using silicone gasket o-rings. Eleven set screws were placed into this upper plate at the locations shown in Figure 9. Eighteen threaded posts (6.4 mm diameter, 38.1 mm length) were mounted along the perimeter of the aluminum base and topped with nuts and washers to provide a compressive sealing force between each layer. To restrict the amount of compression in the silicone foam, stainless steel shims (800 μm thick) were cut into patterns to reside just outside the silicone foam layer and act as "hard stops" for compression. Six thermocouples were inserted through the edge of the flow cell and compressed between the two silicone foam gaskets, allowing the tips to protrude into the flow chamber (Figure 10). Additional silicone vacuum grease was applied to all layer interfaces to aid in sealing potential leaks once pressurized.

Dye Test. The use of injected dyes for flow visualization is well-known.[19] In this investigation, a dye test was run to verify flow

uniformity and the integrity of fluidic seals prior to running reactants for CdS deposition. The flow chamber was filled with deionized water at room temperature at 31 mL/min. The supply stream was then switched to a solution of black dye. Video cameras were used to record and measure the progression of dye as it crossed the front, middle, and back planes of the substrate region.

Deposition Tests. A 152 × 152 mm commercial soda lime glass substrate (Pilkington TEC-15) with a fluorine-doped tin oxide (FTO) layer was assembled within the flow cell reactor. The flow cell was then fixed to a 9 in. × 9 in.Wenesco hot plate (1100 W) and positioned vertically to remove any bubbles that were introduced during priming.

To deposit the films, the reaction chamber was first circulated with room-temperature deionized water and allowed to reach a steady temperature of 83 °C before switching to reagents. One percent by volume of Triton X-100 surfactant was added to the deionized water to

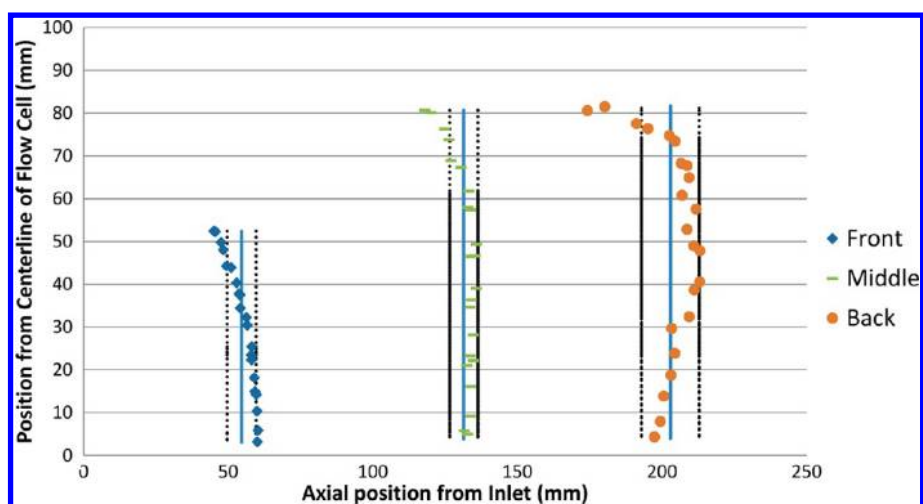**Figure 7.** Standard deviations of flow fronts for deflected-plate channel profiles roughly 600 μm high along the flow cell centerline and 800 μm high along the edge of the flow cell for front plane = 5.0 mm; middle plane = 4.9 mm; and back plane = 10.0 mm (shows half of flow field from center axis).
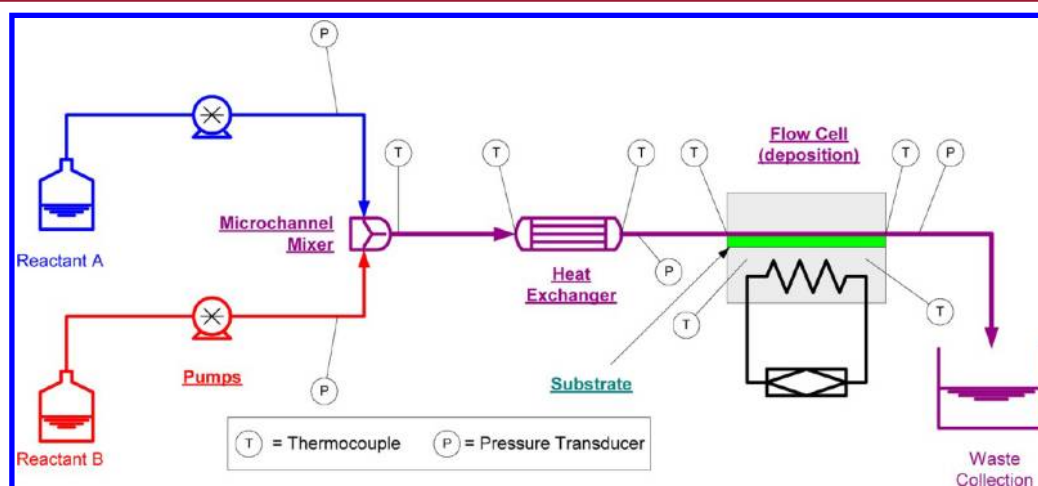

Figure 8. Test stand schematic for 152 × 152 mm CdS deposition. Data acquisition and control system are not shown.
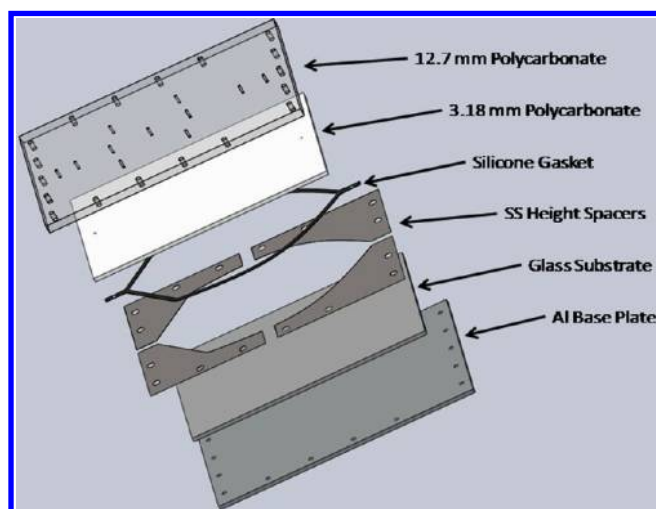

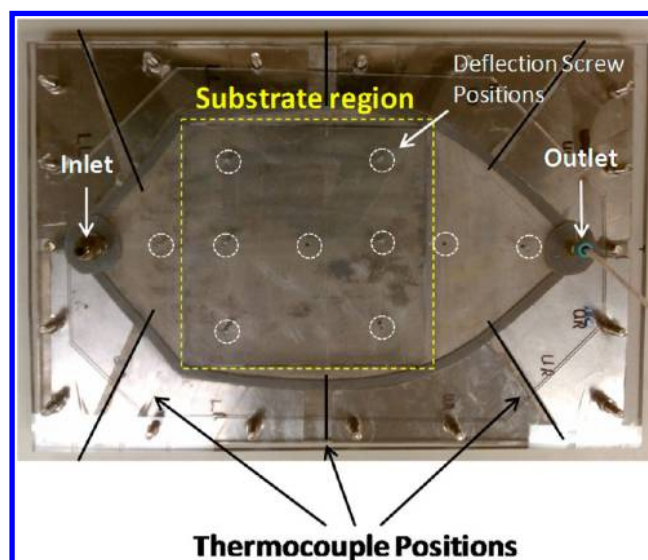**Figure 9.** Flow cell assembly.

Figure 10. Thermocouple and deflection screw positions.

help remove bubbles entrained during priming. Reagents were premixed within two vials marked A and B, with A containing 0.004 M $CdCl_2$, 0.41 M NH_4OH, and 0.04 NH_4Cl, and B containing 0.04 M thiourea. Equal flow rates (15.5 mL/min) of reagents were supplied to the micromixer before entering the thermally insulated microchannel heat exchanger.

The temperature in the heat exchanger was monitored. Induction time after heating was 1 min. The overall deposition time was 5 min, after which all heaters were turned off and the reagent supply was switched

back to deionized water. The system was allowed to flush until the preheater temperature reduced to <40 °C, at which time the pumps were turned off and the flow cell chamber was drained through the inlet connector. The top cover of the flow cell was then removed, and the substrate was rinsed again with deionized water to wash away any noncohesive particulates.

Film Thickness Measurement. Film thickness and uniformity were measured by exploiting the optical properties of CdS at a wavelength of 500 nm. The relationship of film thickness (t) and transmission (T) can be expressed as

$$T = e^{-\alpha t} \tag{1}$$

where the absorption coefficient ($\alpha = 143005.31$ cm^{-1}) was calculated by averaging the values obtained from eq 1. Various CdS films were deposited, as explained elsewhere,[14] and used for calibration of the measurement technique. Film thickness (t) was determined by cross-sectioning the films using a focus-ion-beam (FIB) lift-out process and measuring the cross-sectional thickness of the film using transmission electron microscopy (TEM). Figure 11 shows one of the TEM cross
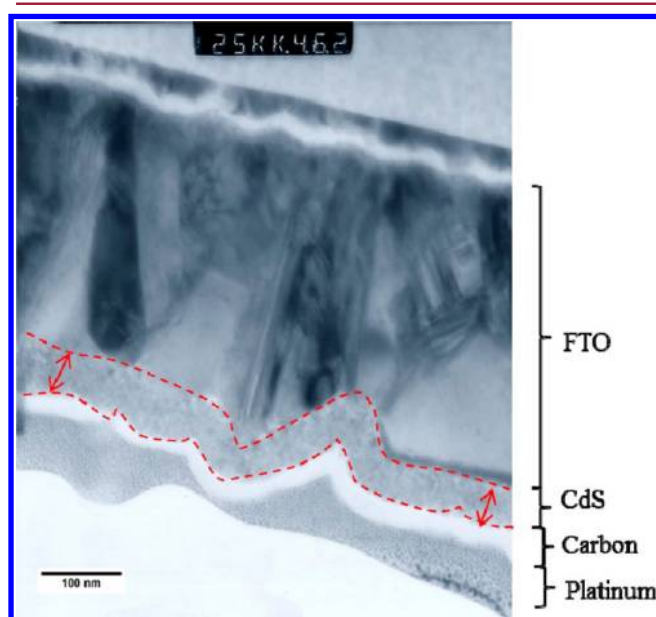

Figure 11. Example TEM cross section used in calibrating the spectrophotometer-based film thickness measurement technique.

sections at 125 000×, including the entire CdS/FTO structure. The CdS layer is between the FTO film and a carbon film. The carbon and platinum layers on top of the CdS layer were added to prevent surface charge accumulation and to introduce a protection layer during the focused-ion-beam (FIB) milling process. This micrograph shows that the FTO layer on the substrate is rough and the CdS layer on top is conformal.

Figure 12 shows the calibration curve of optical thickness determined by the 500 nm transmission model (eq 1) versus physical thickness measured by the FIB/TEM technique. Each data point represents the optical and physical thickness of a CdS film produced using the specified deposition time.

■ RESULTS AND DISCUSSION

Dye Tests. The CFD models for the flow cell were found to be capable of predicting results similar to observations seen in the physical dye tests at 31 mL/min (Figure 13). The distinctive parabolic flow profile is apparent under parallel-plate (PP) conditions, whereas a more uniform profile is seen under deflected-plate (DP) conditions. Statistical comparison of the baseline PP and the DP flow cells is shown in Table 1.
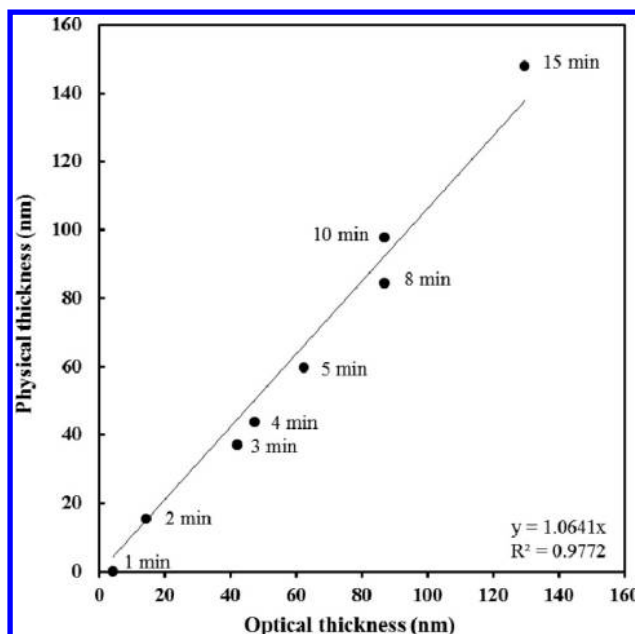

Figure 12. Calibration curve of optical thickness determined using a UV–vis transmission model at 550 nm vs physical thickness determined by FIB cross-sectioning and TEM imaging.
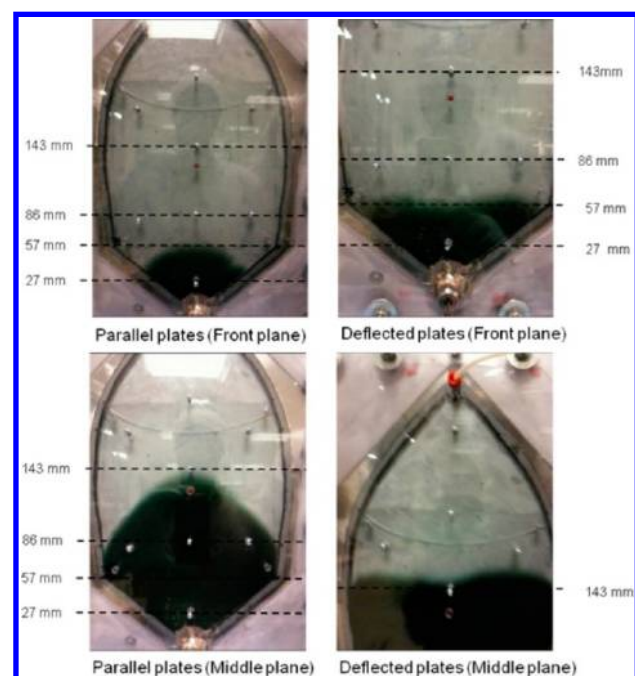

Figure 13. Dye test to assess visual flow distribution at 31 mL/min: (left) parallel-plate flow cell and (right) deflected-plate flow cell.

Results show that the DP method significantly reduced dispersion in the flow front at the front, middle, and back plane of the substrate. CFD results typically underpredicted the flow front dispersion by an average 18.5%, which shows good agreement with the experimental data. This underprediction may be an artifact of axial diffusion, which was not adequately accounted for within the model. For both flow cells, the standard deviation of the axial position steadily increased as each successive plane was crossed. For the parallel-plate flow cell, the standard deviation almost tripled during both CFD modeling and the dye test. For the deflected-plate flow cell, the standard deviation is

Table 1. Comparison of Flow Front Uniformity Measured by the Standard Deviation of the Axial Position of Tracer Particles (CFD) and Dye (Experimental) as a Percentage of the Substrate Size (152 mm)[a]

	front (57.5 mm)[b]	middle (143.1 mm)[b]	back (228.6 mm)[b]
no deflection (CFD)	5.16%	12.33%	16.97%
no deflection (dye)	7.63%	11.63%	22.16%
change	2.47%	−0.70%	5.19%
% error	32.37%	−6.02%	23.43%
200 μm deflect (CFD)	3.36%	3.25%	6.65%
200 μm deflect (dye)	3.88%	4.83%	7.83%
change	0.52%	1.58%	1.18%
% error	13.44%	32.74%	15.11%

[a]Standard deviation [% of substrate size (152 mm)]. [b]Axial distance from inlet.
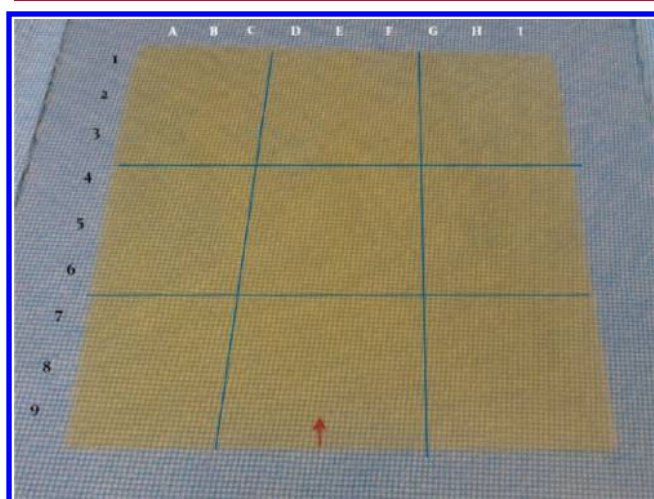

Figure 14. Example of a 9 × 9 labeling system used for measuring film thickness points. The film shown was produced using the deflected-plate flow cell at 31 mL/min.

consistently one-third to one-half the level of dispersion in the parallel-plate flow cell. An increase in standard deviation on the back plane of the deflected-plate flow cell was seen both in CFD (see Figure 7, right) and experimentally (dye). This may be due to over-restriction of the axial channel height toward the back plane, suggesting that additional optimization of the flow profile is possible.

Deposition Tests. For the final set of deposited films, characterization involved dividing the substrate into regions and labeling the regions by column and row for consistent comparison. Figure 14 shows an example labeling scheme used for recording data consisting of nine cells each having nine subcells (three rows and three columns). Initially, a total of 45 data points were collected to evaluate the uniformity of the coating consisting of data for the four corner subcells and one center subcell for each cell. For each film, additional analysis was performed to determine what resolution of data points was needed to adequately characterize the film. In general, it was determined that 6 × 6 data points significantly changed the film uniformity compared to the 45 data points, whereas 8 × 8 data points and beyond did not significantly change the film uniformity. Figure 15 shows the final film morphologies as measured using the UV−vis spectroscopic method.

Results suggest that the velocity distribution had a direct impact on the uniformity of the final CdS film. The overall average thickness and standard deviation measured were 25.9 ± 13.5 nm and 21.5 ± 2.6 nm for the PP and DP conditions, respectively. The overall thickness of the final film in the DP experiment showed a greater than 5× reduction in the variability of the film thickness. For PP conditions, it is visually apparent that film growth is thicker in the middle and thinner along the outside of the flow cell. This follows the intuition that the final film would grow more rapidly in the faster flowing center regions where the convective boundary layer is thinner. This is also a region where reactants are replenished at a much faster rate. This increase in deposition rate may also explain why the film produced in the PP flow cell is thicker on average than the film produced in the DP flow cell. Alternatively, differences in average thickness also could be due to the shorter residence time for reactants in the DP flow cell caused by the higher velocities due to the smaller channel cross section. The actual cross section shown in Figure 16 below shows an axial flow cell channel height of around 400 μm on average. As a rough analysis, assuming that the DP deflection is triangular, the deflection cuts off about one-quarter of the channel cross section, suggesting a decrease in residence time of 25%. The average thickness of the film
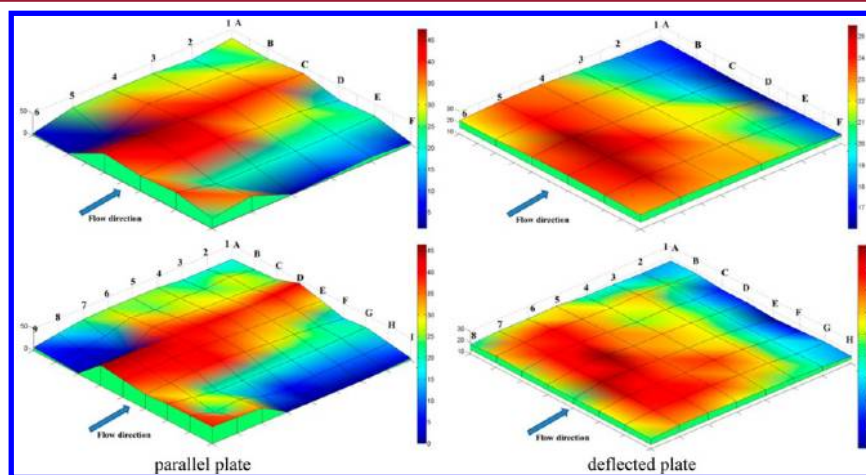

Figure 15. Thickness profile for films produced using parallel-plate (left) and deflected-plate (right) flow cells at 31 mL/min: (top) showing 6 × 6 data point resolution and (bottom) showing enhanced resolution. Arrows show flow direction.
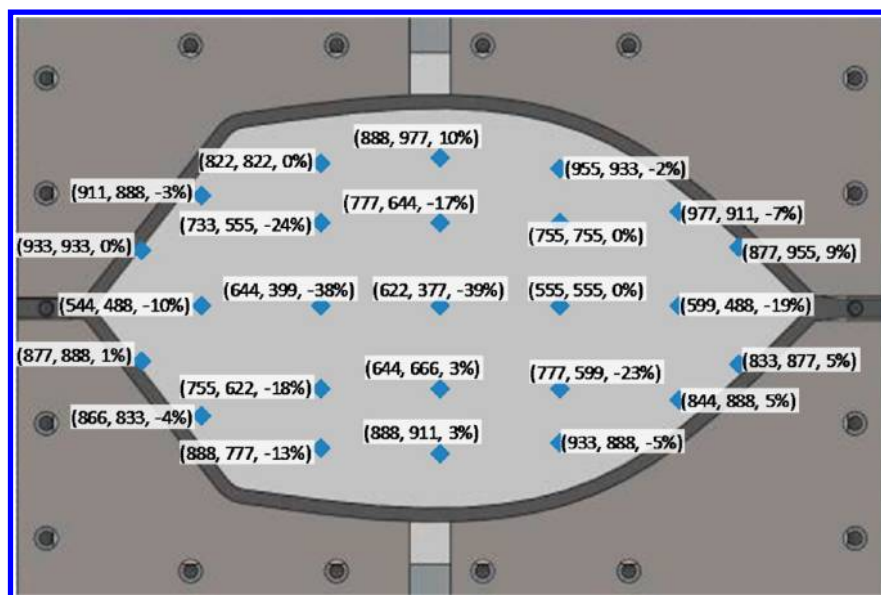
Figure 16. Channel heights in CFD vs measured in experiment using a laser scanning microscope along with percent error.
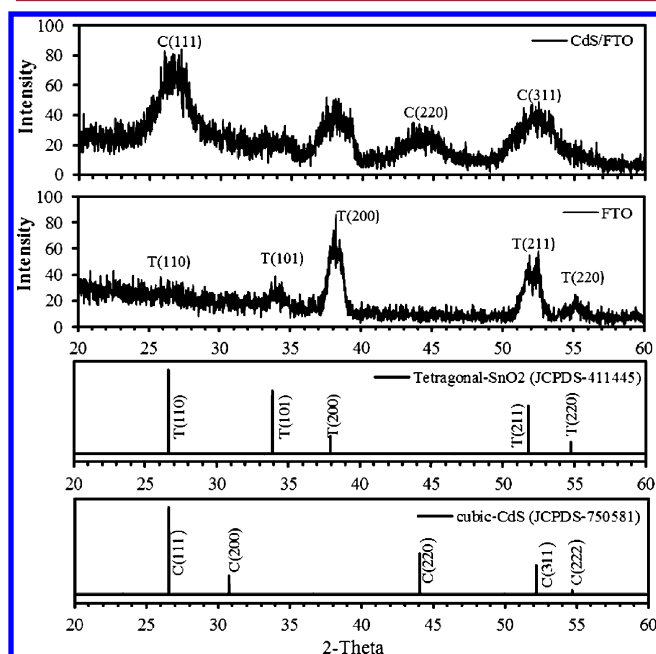

Figure 17. Grazing-incidence X-ray diffraction pattern for the CdS films deposited in a deflected flow cell and the bare FTO substrate.

produced in the DP flow cell is about 83% of the average thickness of the film produced in the PP flow cell. Consequently, a 25% change in residence time could easily explain this difference in film thickness, assuming a linear impact on growth rate with residence time.

Of interest in the DP film is the dip in the film thickness toward the back center of the film, which likely caused a considerable amount of the variability in that film. The CFD results for the DP flow cell in Figures 6 and 7 show that the flow distribution is significantly worse for the back plane of the plate. This is largely due to the fact that FEA results and the experimental setup were not able to closely match the desired constant velocity cross sections adjacent to this region. This is demonstrated in Figure 16, which shows a comparison of the CFD and measured channel cross sections within the deflected-plate flow cell. It is likely that

discrepancies in back row dimensions between the experimental and the ideal constant velocity flow cell designs led to higher (double) flow profile deviations for the back row of the flow cell, as shown in Table 1. The suppression of flow in the back center of the flow cell led to a thinner film in that region. This suggests the importance of maintaining a constant velocity through the deposition region of the flow cell. This issue could be ameliorated through the use of a different technique to implement the deflected cross section. One such technique could be to machine the deflected profile into the upper plate rather than to use plate mechanics.

Adding to this problem is the fact that, in Figure 15 (right), the back row of measurements all show lower thicknesses. This suggests that the deposition rate is slower toward the back of the flow cell. Possible reasons for this could be a higher concentration of byproducts impeding mass transfer of reactants or simply depletion of reactants. Of further interest toward the back of the substrate is the fact that the edges of the film are thinning before the center axis of the film. The flow path along the side of the flow cell is longer than the flow path down the axis of the flow cell. This could be further evidence for the depletion of reactants.

Material Characterization. Figure 17 shows grazing-incidence (0.5°) X-ray diffractograms (Bruker D8 Discover, Cu Kα = 1.54056 Å) of the bare FTO substrate and the CdS film deposited by the deflected-plate flow cell. All peaks from the bare FTO layer index match exactly to tetragonal SnO_2 (JCPDS-411445). The CdS film shows peaks at 26.45, 43.78, and 51.96°, which match well with C(111), C(220), and C(311) of cubic CdS (JCPDS-750581).

■ CONCLUSIONS

In this paper, a 152 × 152 mm deflected-plate flow cell for the microreactor-assisted solution deposition (MASD) of CdS was developed that increased film thickness uniformity by over 5 times for continuous flow deposited films. Final film thicknesses of 21.54 ± 2.64 nm were achieved. This level of film uniformity compares favorably with prior continuous flow cell microreactors for solution deposition showing over 5× variation in chemical product (nanowire) dimensions over a 30 mm dimension.[8] This

improvement was achieved by addressing the problems of flow distribution within the high-aspect-ratio flow cell through deflection of the top plate. It is expected that this technique could open the use of MASD as a technique to produce large area films using short-life intermediate chemistries. As a solution deposition method, MASD holds the potential to deposit films at lower temperatures than traditional PVD and CVD methods without the need for vacuum. To further improve film uniformity for films deposited in the MASD flow cell, greater precision is needed in creating the deflection profile of the flow cell, and efforts are needed to manage the depletion of reactants in the axial direction.

■ **AUTHOR INFORMATION**

Corresponding Author
*E-mail: brian.paul@oregonstate.edu.

Present Address
‖Barr Engineering Co., Hibbing, MN.

Notes
The authors declare no competing financial interest.

■ **REFERENCES**

(1) Shafarman, W. N.; Siebentritt, S.; Stolt, L. Cu(InGa)Se$_2$ Solar Cells. In *Handbook of Photovoltaic Science and Engineering*; Luque, A., Hegedus, S., Eds.; Wiley: Chichester, U.K., 2011; Chapter 13.

(2) Orgassa, K.; Rau, U.; Nguyen, Q.; Schock, H. W.; Werner, J. Role of CdS buffer layer as an active optical element in Cu(In,Ga)Se$_2$ thin-film solar cell. *Prog. Photovoltaics* **2002**, *10*, 457−463.

(3) Chopra, K. L.; Paulson, P. D.; Dutta, V. Thin-film solar cells: An overview progress in photovoltaics. *Prog. Photovoltaics* **2004**, *12*, 69−92.

(4) Chang, Y. J.; Mugdur, P. H.; Han, S. Y.; Morrone, A. A.; Ryu, S. O.; Lee, T. J.; Chang, C. H. Nanocrystalline CdS MISFETs fabricated by a novel continuous flow microreactor. *Electrochem. Solid-State Lett.* **2006**, *9*, G174−G177.

(5) Chang, Y. J.; Su, Y. W.; Lee, D. H.; Ryu, S. O.; Chang, C. H. Investigate the reacting flux of chemical bath deposition by a continuous flow microreactor. *Electrochem. Solid-State Lett.* **2009**, *12*, 244−247.

(6) Mugdur, P.-H.; Chang, Y.-J.; Han, S.-Y.; Morrone, A. A.; Ryu, S.-O.; Lee, T. J.; Chang, C.-H. A comparison of chemical bath deposition of CdS from a batch reactor and a continuous flow microreactor. *J. Electrochem. Soc.* **2007**, *154*, D482−D488.

(7) Dona, J. M.; Herrero, J. Chemical bath deposition of CdS thin films: An approach to the chemical mechanism through study of the film microstructure. *J. Electrochem. Soc.* **1997**, *144*, 4081−4091.

(8) McPeak, K.; Baxter, J. ZnO nanowires grown by chemical bath deposition in a continuous flow microreactor. *Cryst. Growth Des.* **2009**, *9*, 4538−4545.

(9) McPeak, K.; Baxter, J. Microreactor for high-yield chemical bath deposition of semiconductor nanowires: ZnO nanowire case study. *Ind. Eng. Chem. Res.* **2009**, *48*, 5954−5961.

(10) Chung, B. J.; Robertson, A. M.; Peters, D. G. The numerical design of a parallel plate flow chamber for investigation of endothelial cell response to shear stress. *Comput. Struct.* **2003**, *81*, 535−546.

(11) Hung, P. J.; Lee, P. J.; Sabounchi, P.; Aghdam, N.; Lin, R.; Lee, P. L. A novel high aspect ratio microfluidic design to provide a stable and uniform microenvironment for cell growth in a high throughput mammalian cell culture array. *Lab Chip* **2005**, *5*, 44−48.

(12) Amador, C.; Gavriilidis, A.; Angeli, P. Flow distribution in different microreactor scale-out geometries and the effect of manufacturing tolerances and channel blockage. *Chem.—Eng. J.* **2004**, *101*, 379−390.

(13) Griffini, G.; Gavriilidis, A. Effect of microchannel plate design on fluid flow uniformity at low flow rates. *Chem. Eng. Technol.* **2007**, *30*, 395−406.

(14) Balaji, S.; Lakshminarayanan, S. Improved design of microchannel plate geometry for uniform flow distribution. *Can. J. Chem. Eng.* **2006**, *84*, 715−721.

(15) Bakker, D. P.; Plaats, A.; Verkerke, G. J.; Busscher, H. J.; van der Mei, H. C. Comparison of velocity profiles for different flow chamber designs used in studies of microbial adheasion to surfaces. *Appl. Environ. Microbiol.* **2003**, 6280−6287.

(16) Commenge, J. M.; Falk, L.; Corriou, J. P.; Matlosz, M. Optimal design for flow uniformity in microchannel reactors. *AIChE J.* **2002**, *48*, 345−357.

(17) Pan, M.; Tang, Y.; Pan, L.; Lu, L. Optimal design of complex manifold geometries for uniform flow distribution between micro-channels. *Chem.—Eng. J.* **2008**, *137*, 339−346.

(18) Ramprasad, S.; Wei-Su, Y.; Chang, C.; Paul, B. K.; Palo, D. R. Cadmium sulfide thin film deposition: A parametric study using microreactor-assisted chemical solution deposition. *Sol. Energy Mater. Sol. Cells* **2012**, *96*, 77−85.

(19) Sinton, D. Microscale flow visualization. *Microfluid. Nanofluid.* **2004**, *1*, 2−21.